Supplementary Materials A. Table showing reasons and amounts for removal of half-hourly eddy covariance CH_4 flux data

	Measurements remaining (% remaining)		
Reason	North (flooded)	Central (drained)	South (int)
Non-filtered data	3072 (100%)	2112 (100%)	768 (100%)
Technical downtime	2997 (98%)	1995 (94%)	715 (93%)
Heavy fog, mist, rain, snow	1634 (53%)	1041 (49%)	529 (69%)
Winds outside the footprint	1148 (37%)	697 (33%)	434 (57%)
Low turbulence or stationarity	698 (23%)	559 (26%)	224 (29%)

Supplementary Materials B. Reconstructed water table and thawing/freezing dynamics

Equation B1 shows the empirical 1-dimensional water balance model used to extend water table measurements from the growing season into the autumn (text Fig. 2).

$$WT_t = WT_{t-1} + \frac{a\Delta precip + b\Delta pumped - c\Delta ET_{pot} - d\dfrac{WT_{t-1}+20}{TD_{t-1}} + e}{por(WT_{t-1})} \quad \text{(B1)}$$

where Δ denotes the change in the specified variable between the previous and present steps, a subscript t denotes the present step and a subscript t-1 denotes the previous step, *WT* is the water table height above the surface (cm), *precip* is precipitation (cm) adjusted for undercatch according to Yang et al. (1998), *pumped* is the water added or removed through pumping (cm), ET_{pot} is the potential evapotranspiration (cm), *TD* is the thaw depth (cm), $por(WT_{t-1})$ is the porosity of the soil as a function of water table position in the previous step, and *a*, *b*, *c*, *d*, and *e* are fitted constants. Potential evapotranspiration was calculated according to the Penman-Monteith equation (Monteith and Unsworth, 1990) and by using the Water Balance Simulation Model ETH (WaSiM-ETH) (Liljedahl, 2011; Schulla, 1997; Schulla and Jasper, 2007). Potential evapotranspiration showed very good agreement with actual evapotranspiration (Liljedahl, 2011) and removed the need to gap-fill eddy covariance measurements. We used a soil porosity function interpolated from Hinzman et al. (1991).

Table B1. Fitted coefficients for empirical water table model

Coefficient	*a*	*b*	*c*	*d*	*e*	RMSE
North	2.2	0.75	1.27	0.04	0.02	0.5 cm
Central	2.8	0	1.9	0.49	0.31	0.9 cm
South	2.56	10.7	2.6	0.10	0.07	0.2 cm

Fitting our empirical model yielded reasonable and generally consistent coefficients with small root mean square errors (Table B1; $R^2 > 90\%$; $p < 0.001$) and unbiased estimates (Fig. B1). Reconstructed water table heights for the Central (drained) section using Eq. B1 also showed good agreement in magnitude and behaviour to independently estimated water table

heights derived from the relationship between water table and soil moisture in the top 10 cm (text Fig. 2a) until the water table approached the surface and the relationship became unreliable. Our modelling results for the North (flooded) and South (intermediate) sections could not be verified in this manner as the moisture sensors in these sections remained inundated throughout the autumn.

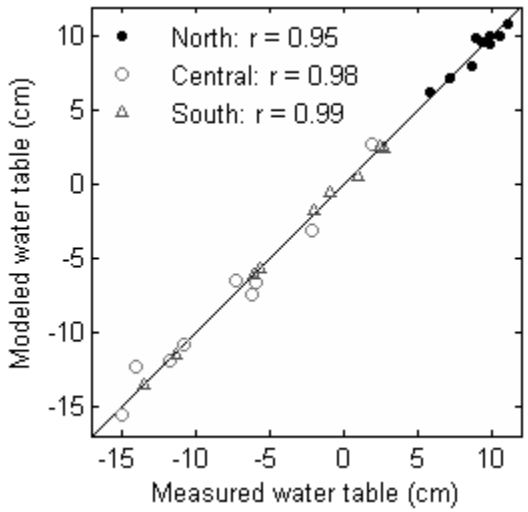

Figure B1. Measured vs. modelled water table positions compared to a 1:1 relationship.

Prior to the onset of refreezing in the active layer, average thaw depths for all manipulation sections were reconstructed (text Fig. 3) using ground heat flux measurements. The relationship between cumulative ground heat flux and thaw depth during the growing season showed a linear relationship after thaw surpassed 15 cm (Fig. B2). This relationship was used to extend the thaw depth measurements until 19 September, when the cumulative ground heat flux reached its maximum and reversed direction. This date also corresponded with the decline in surface temperature below 2 °C, which Romanovsky and Osterkamp (1997) showed to be the point at which thawing stops and refreezing begins from the bottom-up. The increase in thaw between the last measured thaw depth on 19 August and 19 September was < 5 cm for all three sections, which was similar to the increase in thaw depth between late August and mid-September observed at this site in 2007 (Y. Kim, unpublished data).

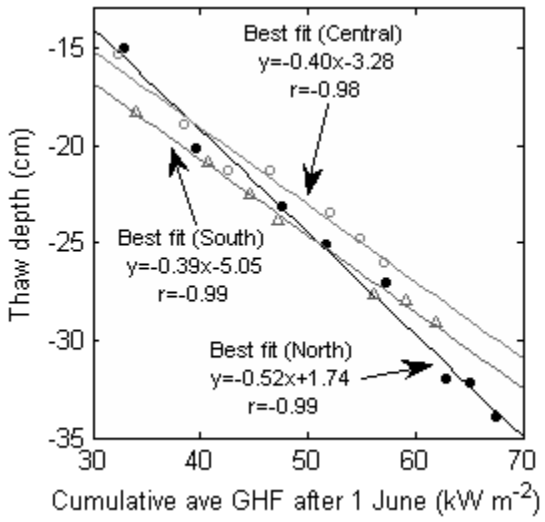

Figure B2. Relationships between cumulative average ground heat flux (GHF; cumulative average of five sensors each) and thaw depth (b) used to simulate thaw depth from 19 August to 21 September.

After 19 September the top-down and bottom-up freezing fronts were reconstructed for the North (flooded) and Central (drained) sections (text Fig. 3) using soil temperature profiles (text Fig. 4a and b) and interpolating between the dates at which the soil temperature at a specific depth dropped consistently below 0 °C. We did not reconstruct South (intermediate) freezing fronts due to the absence of flux data after 7 September. The maximum thaw depth on 19 September was used as the starting point for bottom-up freezing. Following observations by Osterkamp and Romanovsky (1997), we assumed that 35% of the active layer froze from the bottom up. This was consistent with our temperature profile and soil moisture measurements. For example, soil temperatures at 20 cm and 30 cm depth in the North (flooded) section dropped below 0 °C at the same time (text Fig. 4a) and soil moisture in the 20-30 cm depth range began a slow decline at this point (text Fig. 4c), indicating that the freezing fronts met somewhere between these two soil layers (20 and 30 cm). This was consistent with a depth of 24.6 cm estimated assuming that 35% of the active layer froze from the bottom-up. For the Central (drained) section, freezing from the bottom-up was calculated to reach a depth of 18.9 cm. This was consistent with a nearly immediate decline in unfrozen soil moisture in the 20-30 cm depth range at the onset of top-down soil freezing, and a much lower value when the soil temperature at 20 cm depth declined below 0 °C (text

Fig. 4d). Therefore we used the soil temperature at 20 cm depth as an approximate point when the freezing fronts met. We consider the distance between the freezing fronts to be the unfrozen soil thickness, acknowledging that a large amount of unfrozen soil moisture is still present just below 0 °C (Osterkamp and Romanovsky, 1997).

References for Supplementary Materials B

Hinzman, L. D., Kane, D. L., Gieck, R. E., and Everett, K. R.: Hydrologic and thermal-properties of the active layer in the Alaskan Arctic, Cold. Reg. Sci. Technol., 19, 95-110, 1991.

Liljedahl, A. K.: The hydrologic regime at sub-arctic and arctic watersheds: present and projected, Ph. D. dissertation, University of Alaska, Fairbanks, 257 pp., 2011.

Monteith, J. L., and Unsworth, M. H.: Principles of Environmental Physics, Third ed., Academic Press, Burlington, MA, USA, 1990.

Osterkamp, T. E., and Romanovsky, V. E.: Freezing of the active layer on the coastal plain of the Alaskan Arctic, Permafrost Periglac, 8, 23-44, 10.1002/(sici)1099-1530(199701)8:1<23::aid-ppp239>3.3.co;2-u, 1997.

Romanovsky, V. E., and Osterkamp, T. E.: Thawing of the active layer on the coastal plain of the Alaskan Arctic, Permafrost Periglac, 8, 1-22, 10.1002/(sici)1099-1530(199701)8:1<1::aid-ppp243>3.0.co;2-u, 1997.

Schulla, J.: Hydrologische Modellierung von Flussgebieten zur Abschatzung der Folgen von Klimaanderungen (Hydrological modelling of river basins for estimating the effects of climate change), Ph.D. dissertation, Zurcher Geographische Schriften, ETH Zurich, Switzerland, 1997.

Schulla, J., and Jasper, K.: Model description WaSiM-ETH, Internal Report, Institute for Atmospheric and Climate Science, ETH Zurich, Switzerland, 2007.

Yang, D. Q., Goodison, B. E., Ishida, S., and Benson, C. S.: Adjustment of daily precipitation data at 10 climate stations in Alaska: Application of World Meteorological Organization intercomparison results, Water Resour. Res., 34, 241-256, 10.1029/97wr02681, 1998.